Biophysical Chemistry 245 (2019) 25–33

Contents lists available at ScienceDirect

Biophysical Chemistry

journal homepage: www.elsevier.com/locate/biophyschem

Detection of Mg^{2+}-dependent, coaxial stacking rearrangements in a bulged three-way DNA junction by single-molecule FRET

Michael P. Leveille, Thao Tran, Gianna Dingillo, Brian Cannon*

Department of Physics, Loyola University Chicago, Chicago, IL, USA

HIGHLIGHTS

- Stable folding of bulged, three-way DNA junctions depends on the Mg^{2+} concentration.
- The pyrimidine content of the bulge can specify the coaxial stacking arrangement.
- Bulged, three-way DNA junctions can interconvert between the two stacked conformers.

GRAPHICAL ABSTRACT

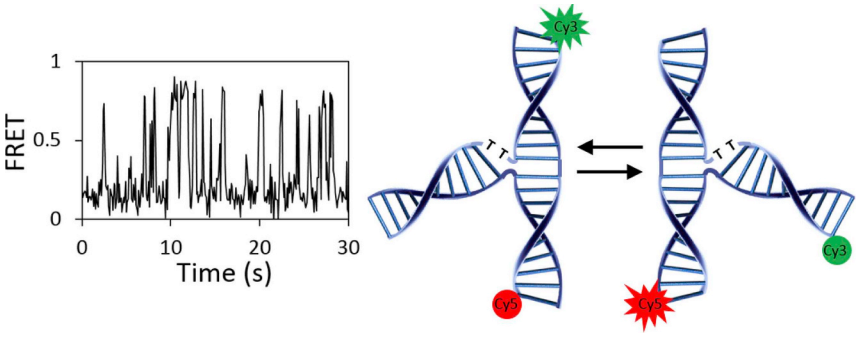

ARTICLE INFO

Keywords:
Three-way junction
Single molecule FRET
DNA conformation
Structural dynamics
Conformers
DNA folding

ABSTRACT

Three-way helical junctions (3WJs) arise in genetic processing, and they have architectural and functional roles in structured nucleic acids. An internal bulge at the junction core allows the helical domains to become oriented into two possible, coaxially stacked conformers. Here, the helical stacking arrangements for a series of bulged, DNA 3WJs were examined using ensemble fluorescence resonance energy transfer (FRET) and single-molecule FRET (smFRET) approaches. The 3WJs varied according to the GC content and sequence of the junction core as well as the pyrimidine content of the internal bulge. Mg^{2+} titration experiments by ensemble FRET show that both stacking conformations have similar Mg^{2+} requirements for folding. Strikingly, smFRET experiments reveal that a specific junction sequence can populate both conformers and that this junction undergoes continual interconversion between the two stacked conformers. These findings will support the development of folding principles for the rational design of functional DNA nanostructures.

1. Introduction

Three-way junctions (3WJs) are common elements in structured RNA molecules and in DNA processing, and they have with a growing number of applications in DNA and RNA nanostructures. These structures serve architectural roles to position and orient helical domains, and the junction cores can have functional roles as sites for ligand binding and catalysis for structured RNAs, including catalytic RNAs [1–3], ribosomal structures [4,5], and viral elements [6]. Although the natural occurrence of DNA 3WJs is limited to recombination [7] and replication events [8], including slip-outs associated with trinucleotide repeat disorders [9], these junctions are components in DNA-based nanostructures [10,11] and are utilized in bioengineering applications, such as protein detectors [12], diagnostic assays [13], and cancer-

Abbreviations: FRET, fluorescence resonance energy transfer; nt, nucleotide; bp, base pair; 3WJ, three-way junction

* Corresponding author at: Department of Physics, Loyola University Chicago, 1032 West Sheridan Road, Chicago, IL 60660-1537, USA.
E-mail address: bcannon1@luc.edu (B. Cannon).

https://doi.org/10.1016/j.bpc.2018.12.001
Received 3 September 2018; Received in revised form 30 November 2018; Accepted 1 December 2018
Available online 05 December 2018

targeting therapeutic agents [14].

Fully complementary 3WJs primarily adopt a static, trigonal planar conformation without coaxial stacking [15] and display some flexibility in the relative positioning of the junction arms [16–18]. The presence of single-stranded domains, such as single mismatches, tandem mismatches, bulges, and internal loops, locally destabilize neighboring helical structure [19–23]. Bulges within helical domains can induce a flexible hinge conformation in which the helical domains becomes increasingly bent as the size of the bulge expands [24–26]. The insertion of an internal bulge within the 3WJ core has profound effects on its folding as it expands the conformational capabilities of DNA and RNA junctions [6,27–33]. In the absence of divalent metal ions, bulged 3WJs can sample multiple conformations that have nanosecond lifetimes and can regulate interhelical charge transport through the junction [34,35]. In the presence of divalent metal cations, which stabilize structure formation in nucleic acids, bulged 3WJs can fold into two coaxially stacked arrangements (conformers) that differ in terms of the identities of the stacked domains and the polarity of the bulge strand [28,32]. The sequence and local organization in the 3WJ core specifies conformer selection [29]. Experimental observations suggest that 3WJs predominantly favor a single conformer, although structural and electrophoretic studies of bulged 3WJs have proposed that some 3WJ sequences may fold into both conformers [29,36,37]. This folding behavior of DNA 3WJs would seemingly contrast with the behavior of DNA four-way junctions (4WJs), which can be mobile and readily undergo structural transitions between different coaxial stacking arrangements of its four helical domains [38–42].

Single-molecule methods have proved effective to detect transient intermediates and provide discrete signals for asynchronous biomolecular events, such as DNA·protein interactions [43,44], conformational changes in structured nucleic acids [39,45], and catalysis [46]. These methodologies have significantly advanced the understanding of the folding principles that govern the formation and dynamics of structured nucleic acids [39,46,47]. Specifically, single-molecule fluorescence resonance energy transfer (smFRET) serves as a spectroscopic ruler that can measure nanometric changes in interdomain distances in real time with millisecond time resolution. For smFRET measurements, the fluorescent dyes Cy3 and Cy5, which function as a FRET pair with Cy3 as the donor and Cy5 as the acceptor in the non-radiative energy transfer mechanism, are incorporated into specific locations within individual biomolecules for concurrent imaging of two fluorescent signals from individual immobilized molecules [48]. The work here presents the first reported application of smFRET to examine the folding of bulged, DNA 3WJs. Using a combination of ensemble FRET and smFRET approaches, the Mg^{2+}-dependent folding for a series of 2-nt bulged, DNA 3WJs with varying core sequences and bulge compositions was studied. The fluorescently labeled 3WJ constructs produce two distinct FRET populations that are consistent with two coaxially stacked conformers. Although most of the junctions fold into a single, static conformer, one notable sequence measurably populates both conformers and displays stochastic transitions between the two conformer states. In addition, the pyrimidine content of the bulge influences the conformer preference. These findings demonstrate that bulged DNA 3WJs can exhibit sequence-dependent, structural dynamics similar to other branched DNA structures.

2. Materials and methods

2.1. Materials and 3WJ sequences

All oligonucleotides were purchased from Integrated DNA Technologies, Inc. (Coralville, IA) with HPLC purification. The concentrations of all oligonucleotides were determined from the 260-nm absorbance values by UV spectrophotometry using the single-stranded extinction coefficients. Each 3WJ was assembled from three oligonucleotide strands: *a*, *b*, and *T*. To reduce the number of oligonucleotides for assembly of the junctions, the distal end of domain B relative to the junction is terminated by a CTTG hairpin loop. Strands *a* and *b* contain domains A and C and domains A, B, and C, respectively, for the 3WJ constructs. The tether strand (*T*) for immobilization is complementary to a 14-bp tethering domain within the *b* strand. The *T* strand is 5′ labeled with the fluorescent dye Cy3 and 3′ biotinylated. The *b* strand is 5′ labeled with the fluorescent dye Cy5. The following sequences were used:

T: 5′-/Cy3/GGGATATCGCGATTCTGCTGTACG/biotin-3′.
J1a: 5′-AATCGCGATATCCCTTCTCATAGCCTACCCCCGCTGTAGC/Cy5–3′.
J1b: 5′-GCTACAGCGGGGCGTCGCATCGTCTTGACGATGCGACGTTGTAGGCTATGAG-3′.
J3a: 5′-AATCGCGATATCCCTTCTCATAGCCTAGCGCCGCTGTAGC/Cy5–3′.
J3b: 5′-GCTACAGCGGCGCGTCGCATCGTCTTGACGATGCGACGTTCTAGGCTATGAG-3′.
J5a: 5′-AATCGCGATATCCCTTCTCATAGCCTACCACCGCTGTAGC/Cy5–3′.
J5b: 5′-GCTACAGCGGTGCGTCGCATCGTCTTGACGATGCGACGTTGTAGGCTATGAG-3′.
J8a: 5′-AATCGCGATATCCCTTCTCATAGCCTGCCACCGCTGTAGC/Cy5–3′.
J8b: 5′-GCTACAGCGGTGCGTCGCATCGTCTTGACGATGCGACGAAGCAGGCTATGAG-3′.
J11a: 5′-AATCGCGATATCCCTTCTCATAGCCTGCCACCGCTGTAGC/Cy5–3′.
J11b: 5′-GCTACAGCGGTGCGTCGCATCGTCTTGACGATGCGACGTTGCAGGCTATGAG-3′.
J12a: 5′-AATCGCGATATCCCTTCTCATAGCCTGCCACCGCTGTAGC/Cy5–3′.
J12b: 5′-GCTACAGCGGTGCGTCGCATCGTCTTGACGATGCGACGGCAGGCTATGAG-3′.

2.2. Sample preparation for ensemble and smFRET experiments

For the ensemble FRET experiments, the 3WJs were assembled by annealing equimolar concentrations of the three strands (*a*, *b*, and *T*) for a final 3WJ concentration of 10 μM. The annealing conditions were 50 mM Tris-Cl (pH 8.0), 50 mM NaCl, and 10 mM $MgCl_2$. The samples were heated to 95 °C in a thermocycler for two minutes and slowly cooled to room temperature. Stepwise assembly of the 3WJs was confirmed by 5% agarose gel electrophoresis (89 mM Tris, 89 mM boric acid, 2 mM EDTA, pH 8.3) with SYBR Green I staining.

For the smFRET experiments, the 3WJs were assembled by annealing the appropriate strands at a *a*:*b*:*T* strand ratio of 3:9:1 in which the *T* strand concentration was 1 μM. The annealing conditions were 50 mM Tris-Cl (pH 8.0), 50 mM NaCl, and 10 mM $MgCl_2$. The samples were heated to 95 °C in a thermocycler for two minutes and slowly cooled to room temperature.

2.3. Steady-state fluorimetry

For the ensemble FRET experiments, the final 3WJ concentration for the samples during the measurements was 10 nM. The measurement conditions were 25 mM Tris-Cl (pH 8.0) and the indicated Mg^{2+} concentration. For the Mg^{2+}-free measurements, 1 mM EDTA was included in the solution to chelate free Mg^{2+}. The data were acquired with a PTI Quantamaster 400 (Horiba Scientific) using quartz cuvettes at 25 °C. The excitation wavelength was 515 nm with an emission scan from 560 to 750 nm. Excitation and emission intensity corrections were applied, and background was acquired from a 10-s scan. The FRET efficiency (E_{FRET}) was calculated using the $(ratio)_A$ method [49] as

$$(ratio)_A = \frac{\int_{620}^{750} (\Phi_{Cy5}(\lambda_{ex} = 515) - N * \Phi_{Cy3}(\lambda_{ex} = 515))d\lambda_{em}}{\int_{620}^{750} \Phi_{Cy5}(\lambda_{ex} = 610)d\lambda_{em}}, \quad (1)$$

where $\Phi_{Cy5}(\lambda_{ex} = 610)$ and $\Phi_{Cy3}(\lambda_{ex} = 515)$ represent the Cy5 and Cy3 fluorescence reference spectra, respectively; $\Phi_{Cy5}(\lambda_{ex} = 515)$ is the doubly labeled, Cy3,Cy5 fluorescence scan of the sample; N is a scaling factor that matches the Cy3 reference spectrum with that component of the sample spectrum. The FRET efficiency (E_{FRET}) is calculated as

$$E_{FRET} = \frac{\varepsilon_{Cy5(610)} * (ratio)_A - \varepsilon_{Cy5(515)}}{\varepsilon_{Cy3(515)}}, \quad (2)$$

The following extinction coefficients were used: ε_{Cy5} (610 nm) = $9.3 \times 10^4\,M^{-1}\,cm^{-1}$, ε_{Cy3} (515 nm) = $9.6 \times 10^4\,M^{-1}\,cm^{-1}$, and ε_{Cy5} (515 nm) = $5.6 \times 10^3\,M^{-1}\,cm^{-1}$ [50,51]. Each junction was separately prepared and measured three times. The Mg^{2+}-dependent FRET data were fit to the following two-state model for metal ion-dependent folding according to [6]:

$$E_{FRET} = E_o + \Delta E_{FRET} \frac{K_A[Mg^{2+}]^n}{1 + K_A[Mg^{2+}]^n}, \quad (3)$$

where E_o is the minimum FRET value, ΔE_{FRET} is the change in FRET at saturating Mg^{2+} concentration, $[Mg^{2+}]$ is the magnesium concentration, n is the cooperativity, and K_A is the apparent association constant. The half-maximum Mg^{2+} concentration is calculated as $[Mg^{2+}]_{1/2} = (1/K_A)^{1/n}$. The model parameters were determined from the experimental data by nonlinear regression using OriginPro (OriginLab, Northampton, MA).

2.4. Single-molecule fluorescence microscopy

For the smFRET experiments, the assembled DNA 3WJs were immobilized to quartz slides (Technical Glass, OH) functionalized through successive addition of biotinylated bovine serum albumin (0.5 mg/mL) and streptavidin (0.1 mg/mL). The DNA molecules were immobilized at a tether concentration of 10 pM in 10 mM Mg^{2+} and 25 mM Tris·Cl (pH 8.0). The experiments were performed by prism-based, total internal reflection fluorescence imaging with an Olympus IX-83 inverted microscope using a 60× water objective. The samples were separately excited with 532-nm and 637-nm lasers (Coherent, Santa Clara, CA) to acquire the data and to confirm the presence of the Cy5 dye, respectively. To slow photobleaching, a deoxygenating imaging buffer comprising 25 mM Tris·Cl (pH 8.0), 10 mM Mg^{2+}, 0.8 mM Trolox, 8% glucose, 0.1 mg/mL glucose oxidase, and 0.04 mg/mL catalase was used. Data were acquired at 10 Hz with an Andor iXon DU897 EMCCD (Andor Technologies, Belfast, UK) cooled to −60 °C. The emission signals from the Cy3 and Cy5 dyes were simultaneously collected for each field of molecules by spatial separation onto different regions of the EMCCD through a series of dichroic mirrors (640-nm cutoff; Chroma Technologies, Bellow Falls, VT). The Cy3 and Cy5 emission signals corresponding to each molecule were correlated using an affine transformation previously determined from a control slide coated with fluorescent nanobeads as fiducial markers. The emission intensities for each dye were corrected for local background. Molecules were excluded from additional analysis based on the following criteria: (i) lack of Cy3 or Cy5 dye based on direct excitation of each dye, (ii) large FRET changes resulting from correlated changes in emission of Cy3 and Cy5, and (iii) insufficient total intensity above background. A FRET time trace was calculated for each molecule from the intensity time traces of the Cy3 and Cy5 signals (I_D and I_A, respectively) as

$$FRET(t) = \frac{I_A(t) - \beta I_D(t)}{I_A(t) + I_D(t)}, \quad (4)$$

where β represents the correction factor for the fractional crossover of the Cy3 signal into the Cy5 channel. SmFRET histograms were generated from multiple fields of views and were best fit by Gaussian distributions using Levenberg-Marquardt optimization with OriginPro. Kinetic analysis was performed using a custom, Python-based program. Cumulative, dwell-time histograms were constructed from the measured durations of hundreds of individual transition events. The conformer transition rates, $k_{A/B \to A/C}$ and $k_{A/C \to A/B}$, were then determined from best fits to the dwell-time histograms by the single-exponential rate equation

$$N(t) = N_{total}[1 - \exp(-kt)], \quad (5)$$

where N_{total} is the total number of observed events. The fits were performed using a Levenberg-Marquardt routine for nonlinear least squares minimization.

3. Results and discussion

3.1. Design of 3WJs for fluorescence studies

Bulged 3WJs consist of three helical domains arranged around a branchpoint (i.e., junction core) with an internal, two-nucleotide bulge domain (Fig. 1). In the presence of divalent metal cations, which are critical cofactors in the folding of structured nucleic acids [53], the helical domains can become organized into two possible stacking arrangements. In the A/B conformer (Fig. 1, left side), helical domains A and B are coaxially stacked; while helical domains A and C are coaxially stacked in the A/C conformer (Fig. 1, right side). In addition to dissimilar stacking partners, the conformers differ in the polarity of the bulge domain, which participates in a quasi-hairpin loop that terminates the unstacked domain [27]. Empirically derived rules from experimental studies successfully predict the stacking arrangement for many bulged 3WJs based on their core sequence [29]; however, the folding behavior of several 3WJs remains unclear [37].

Here, fluorescent 3WJ constructs were devised so that each conformer would produce a distinct FRET signal to examine the structural dynamics of bulged 3WJs. Each helical domain in the 3WJs consists of 12 base pairs. A group of modifications were incorporated into the 3WJ constructs to prepare them for fluorescence study and single-molecule imaging. Domain C contains a 14-nt tether binding domain that is complementary to a biotinylated DNA tether for immobilization of the 3WJ constructs for smFRET imaging. The tethering domain is covalently labeled with the donor dye Cy3, and the dye location is proximal to the far terminal end of domain C with respect to the branchpoint. Domain A is 5′ end labeled with the acceptor dye Cy5. With this labeling scheme, the A/B conformer should produce a higher FRET state than the A/C conformer due to the relative positioning of the dye-labeled domains.

The core sequences of the DNA 3WJs examined in the study are shown in Fig. 2 and are largely based on previously studied 3WJs [31,36,54]. J1 shares the same core sequence as TWJ1 with two thymines in the internal bulge at the branch point [31]. Structural studies show this junction adopts the A/B conformer with the unstacked domain C forming a 66° interdomain angle relative to domain A. The stacking arrangement agrees with predictions based on the empirically derived pyrimidine and loop rules [29]. The pyrimidine rule predicts that that the location of the pyrimidine C at the penultimate position in domain A for J1 favors the A/B conformer. The loop rule indicates that the stability of the quasi-hairpin loop 5′-C/TTG-3′ involving the bulge and terminal base pair of domain C also favors the A/B stacked conformation. In contrast, J3, which has the same base content as J1 but two reversed GC base pairs in the A and C domains, forms the A/C stacked conformation, in agreement with predictions based on the reversed penultimate pyrimidine position in the A domain and the stability of the 5'-CTT/G-3′ hairpin involving the bulge and the unstacked B domain [54]. Previous work on 3WJs with the core sequences of J5, J8, and J11 indicate that these junctions may form mixed populations

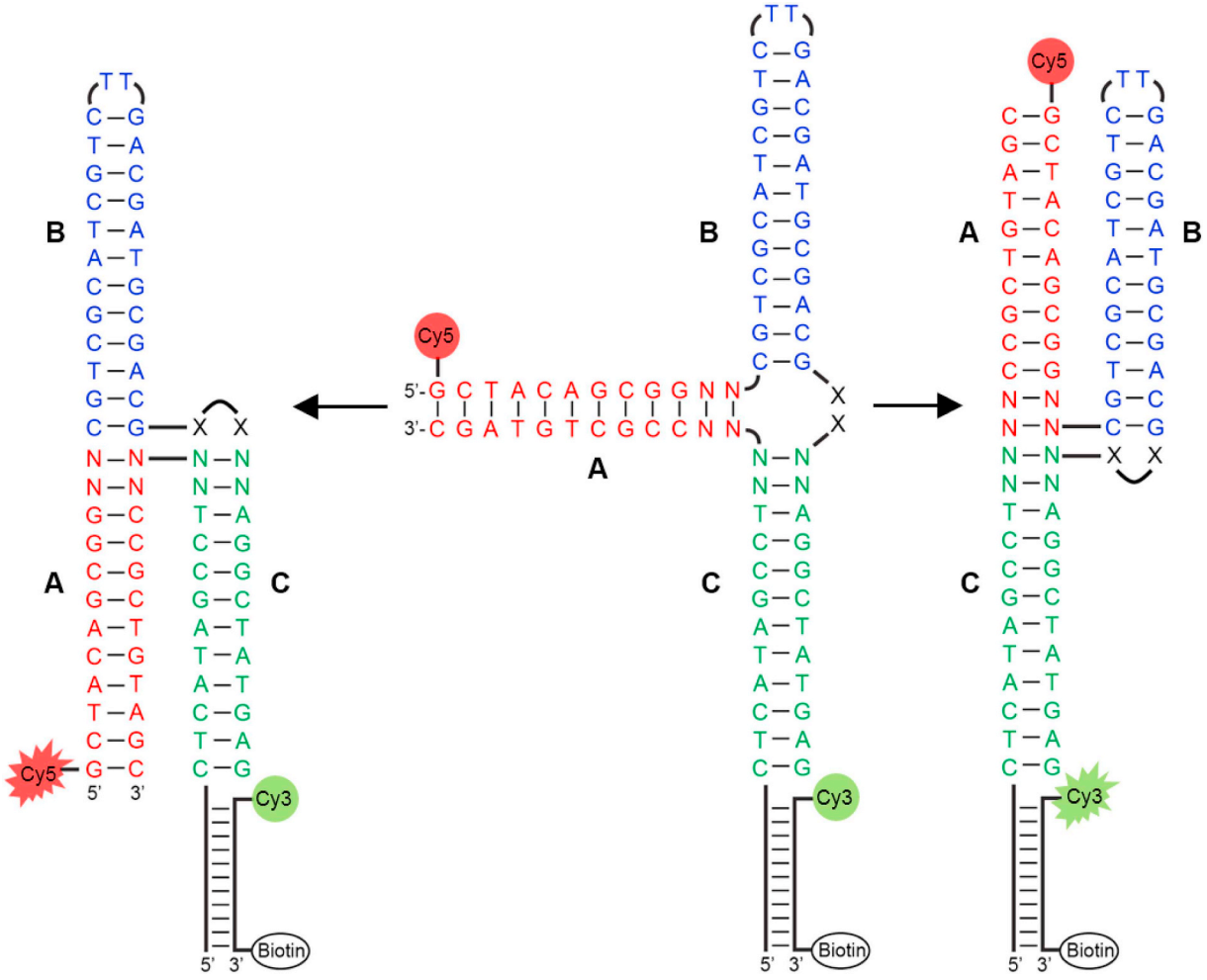

Fig. 1. Secondary structure and labeling scheme for the fluorescently labeled, DNA 3WJs with two-nucleotide bulges. The three helical domains are colored coded as red (domain A), blue (domain B), and green (domain C). The core nucleotides are indicated as N's and the bulge nucleotides are shown as X's. Fig. 2 shows the specific 3WJ core sequences. The central structure represents the open conformation. The left structure corresponds to the A/B stacking conformation. The right structure shows the A/C stacking arrangement. An extension to the C domain is partially complementary to a biotinylated tethering strand that positions the donor dye (Cy3) proximal to domain C. Domain A is labeled with the acceptor dye, Cy5. Each stacking arrangement produces a distinct FRET signal due to the relative positioning of the fluorophore-labeled arms. (For interpretation of the references to colour in this figure legend, the reader is referred to the web version of this article.)

of the A/B and A/C conformers or partially folded states [29,36]. Conformer predictions by the pyrimidine and loop rules do not agree for these sequences. Lastly, J12 has the same junction sequence as J11 but lacks the bulge, serving as a control for the open, unstacked conformation.

3.2. Ensemble FRET studies show Mg^{2+}-dependent, conformer folding for constructs

Divalent metal cation, such as Mg^{2+}, promote folding of structured nucleic acids by minimizing electrostatic repulsion to promote base-stacking interactions. In contrast to 4WJs, which have a metal binding pocket that facilitates folding [55], DNA 3WJs seem to lack a specific metal site, although recent crystal structures identified a metal-binding site in an RNA 3WJ [56]. Using ensemble FRET, the Mg^{2+}-dependent folding curves for J1 and J3 were measured (Fig. 3). In the absence of Mg^{2+}, both junctions have similar FRET efficiencies (E_{FRET}), indicating that the positioning of the arms in the open conformation lacks any significant sequence dependence and is likely in a trigonal planar form. Upon Mg^{2+} addition, E_{FRET} for J1 increases with Mg^{2+} concentration, consistent with this junction folding into the A/B conformer and the interdye distance between the dye-labeled domains decreasing

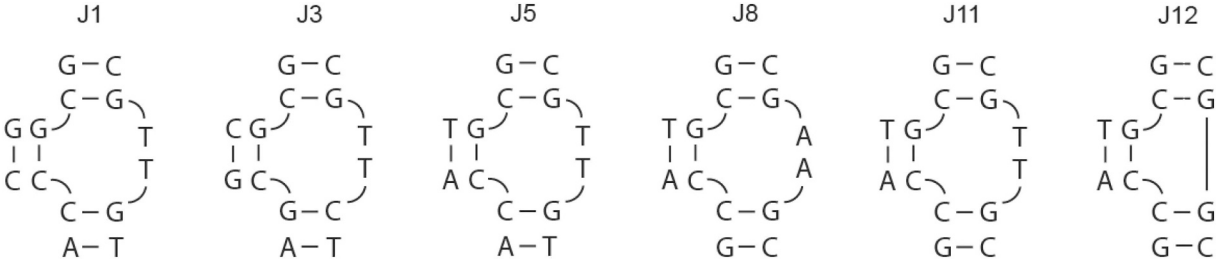

Fig. 2. Secondary structures of the DNA 3WJ cores used for the fluorescently labeled constructs.

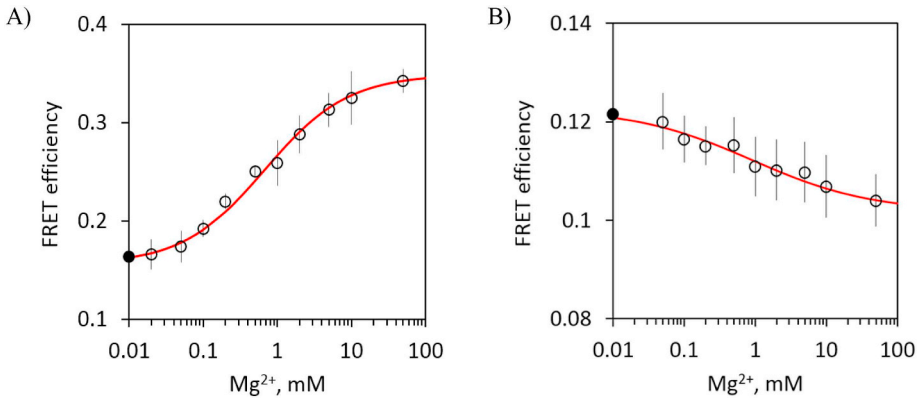

Fig. 3. Ensemble FRET results showing the dependence of the folding of the 3WJs A) J1 and B) J3 on the Mg^{2+} concentration. The solid symbol represents the Mg^{2+}-free measurement. The error bars correspond to standard deviations from three independent measurements. The red line indicates the fit to the data by the two-state model given in Eq. (3) ($R^2 > 0.97$).

(Fig. 3A). In contrast, E_{FRET} for J3 decreases with increasing Mg^{2+}, reflecting formation of the A/C conformer with the dye-labeled domains coaxially stacked (Fig. 3B). Fitting the data with a two-state binding model (Eq. (3)), both junctions have similar half-magnesium concentrations for folding, $[Mg^{2+}]_{1/2}$ = 0.78 and 1.11 mM for J1 and J3, respectively. The Hill coefficients (n) for both junctions are < 1 (0.57 and 0.43 for J1 and J3, respectively), indicating that folding is anti-cooperative and that Mg^{2+}-promoted folding involves diffusely bound metal ions. These experiment confirm that the dye locations on the constructs produce distinguishable FRET signals at saturating Mg^{2+} conditions, consistent with the anticipated conformers for the 3WJs.

3.3. Bulge sequence influences conformer folding

Based on the responses of the dye-labeled 3WJs J1 and J3 to the changes in Mg^{2+} concentration, similar experiments were conducted for the remaining junctions. Table 1 summarizes the E_{FRET} values for all of the 3WJs at saturating Mg^{2+} condition (10 mM Mg^{2+}). The junctions display a range of E_{FRET} values. J5 behaves similarly to J3 with its E_{FRET} value decaying with increasing Mg^{2+} to a similar E_{FRET} as J3. This finding is interpreted as evidence that J5 folds to the A/C conformer. Interestingly, J11 has an intermediate E_{FRET} value (0.197) that falls between the A/B and A/C conformer values, while J8 reaches the same E_{FRET} as J1, indicative of the A/B conformer. J8 and J11 have the same core sequence but differ according to the bulge composition with J11 having a pyrimidine-rich (TT) bulge and J8 having a purine-rich (AA) bulge. This result contrasts with previous findings in which purine/pyrimidine bulge substitutions did not affect the conformer state; however, these junctions had lower GC content for the terminal base pairs in the core than the current study [27]. Considering that thermodynamic studies on duplexes show that A_2 bulges are more destabilizing than T_2 bulges [20,57] and that unpaired purines have higher intrastrand stacking potential than thymines in single-stranded loops [58], the observed differences in the folding behavior for J8 and J11 suggest that the stabilities of the core and loop conformation may be additional factors that influence conformer selection. Lastly, the E_{FRET} values for the fully complementary J12, which lacks a dinucleotide bulge, do not change appreciably from the Mg^{2+}-free value and are intermediate between the values observed for the two stacked conformers, indicating that it remains primarily in the trigonal planar form. Through the ensemble measurements, all of the 3WJ conformations with the exception of J11 could be rationally classified.

Table 1
Summary of steady-state, ensemble FRET values for the 3WJs at saturating Mg^{2+} concentration, 10 mM Mg^{2+}.

3WJ	FRET
J1	0.342 ± 0.027
J3	0.104 ± 0.006
J5	0.111 ± 0.007
J8	0.337 ± 0.032
J11	0.197 ± 0.014
J12	0.171 ± 0.013

3.4. Bulged 3WJs predominantly fold into a single conformation

To probe further into the conformation and structural dynamics of the 3WJs, the junctions were examined by single-molecule FRET at saturating Mg^{2+} conditions(10 mM Mg^{2+}). As a representative example of the A/B conformer, Fig. 4A shows the smFRET time traces for J1, which displays a static, high FRET signal without detectable transitions. Conversely, the trace for J3, as a representative 3WJ for the A/C conformer, has a distinctly lower FRET signal than the J1 trace and similarly does not display any transitions (Fig. 4B). SmFRET histograms were constructed from the accumulated FRET behavior of hundreds of individual 3WJs for the different core sequences. Both A/B conformers, J1 and J8, have unimodal populations with high median FRET values of 0.81 (σ = 0.10) for J1 (Fig. 4C) and 0.82 (σ = 0.09) for J8 (Fig. S1B), based on single-peak Gaussian fits. Similar analysis for the two A/C conformers yielded significantly lower median FRET values, 0.24 (σ = 0.10) for J3 (Fig. 4D) and 0.20 (σ = 0.11) for J5 (Fig. S1A). The fully complementary J12 had a median FRET that was slightly larger than the A/C conformers with a value of 0.32 (σ = 0.09) (Fig. S1C). The findings are consistent with the ensemble FRET experiments in that saturating Mg^{2+} concentration induces the fully folded conformations for the two junctions and that the dye label positions for these constructs generate distinct FRET signals reflecting the organization of the stacked domains. The narrow distributions and absence of detectable transitions indicate that the conformations for these 3WJs are stable states. Treating J1 and J3 as representative examples of the A/B and A/C conformers, respectively, the high FRET peak of J1 is assigned to the A/B conformer, and the low FRET peak of J3 is assigned to the A/C conformer. The ensemble FRET values are systematically lower than the smFRET values. These differences largely arise from the 1) the detection of discrete signals from individual dyes on immobilized molecules compared to the large sample volume for the ensemble measurements and 2) the ability to minimize artefacts (e.g., incomplete junctions, unincorporated dyes, and missing dyes) from the single-molecule data during processing.

The accurate smFRET values were then used to extract structural information about the conformers. FRET changes with interdye distance according to [48]:

$$FRET = \frac{1}{1 + \left(R/R_o\right)^6}, \quad (6)$$

where R_o is the Förster radius of 5.6 nm for the Cy3,Cy5 FRET pair. Although dye orientation and dye linker lengths complicate a strict

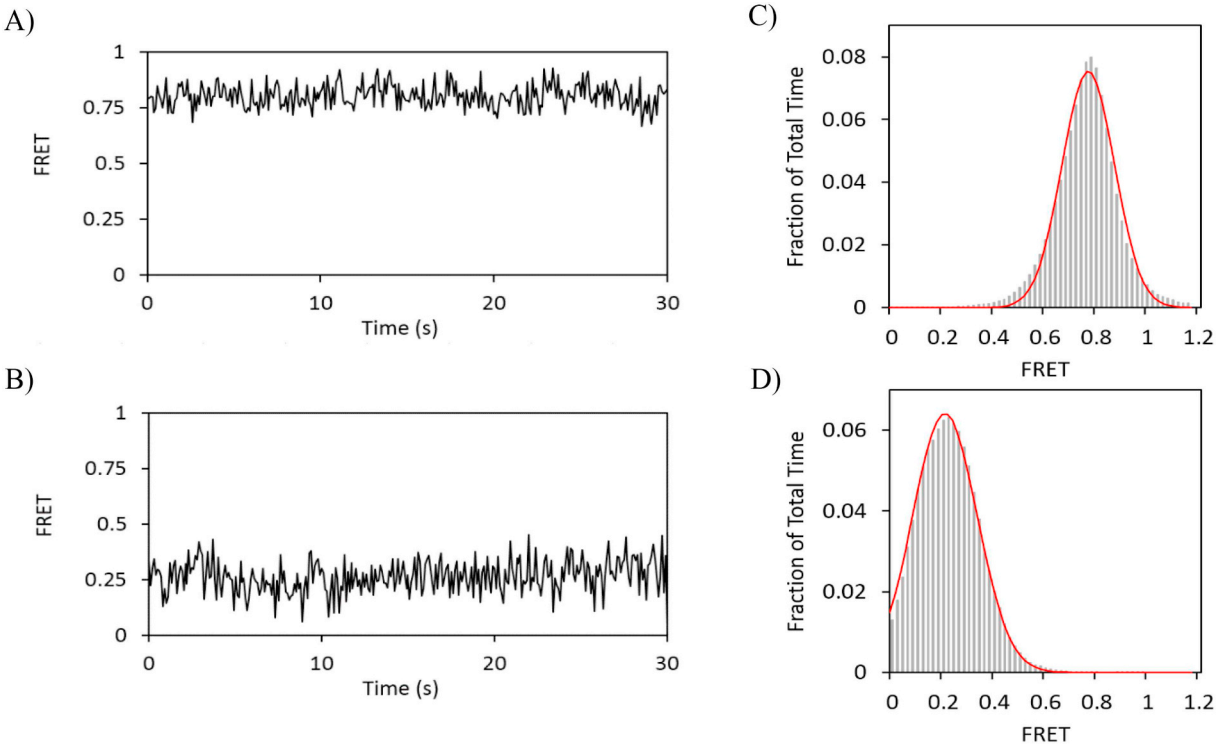

Fig. 4. Single-molecule FRET analysis of DNA 3WJs. Representative FRET time traces for A) J1 and B) J3. The smFRET histograms for C) J1 (N_{mol} = 233) and D) J3 (N_{mol} = 219). The red line represents the single-peak Gaussian fit to the histogram ($R^2 > 0.99$). (For interpretation of the references to colour in this figure legend, the reader is referred to the web version of this article.)

interpretation of the FRET-derived distances, the values from these calculations can provide reasonable estimates of the physical characteristics. For the A/B conformer of J1, the dye-labeled domains A and C are not stacked; therefore, a simple geometric model is invoked with domain C positioned at some interdomain angle (θ) away from domain A with respect to the coaxial stacking axis of domains A and B (Fig. S2). Considering that domains A and C have 12-bp lengths, the FRET-derived, interdye distance of 4.4 ± 0.5 nm yields an interdomain angle of θ = 64 ± 7°, in close agreement with the previously reported value of 66° [29]. Similar analysis for the fully complementary 3WJ, J12, yields an interdomain angle of θ = 102 ± 10°, consistent with the expectation for the trigonal planar conformation. Based on Eq. (6), the median FRET value from J3 for the A/C conformer equates to a distance of 6.7 ± 1.0 nm. This value approximates the expected end-to-end distance of a pair of coaxially stacked, 12-bp DNA helical domains with a pitch of 0.34 nm/bp. The structural information derived from the smFRET data for the two, coaxially stacked conformers agrees with solution structures [54] and validates the conformer interpretations of the smFRET experiments.

3.5. J11 exhibits dynamic transitions between A/B and A/C conformers

The ensemble FRET experiments with J11 indicate that its folding behavior deviates from the static conformers of the other bulged 3WJs, suggesting that J11 adopts multiple conformations or some partially folded state. In contrast to the static behavior observed for the other bulged 3WJs, the smFRET time traces for J11 at 10 mM Mg^{2+} display well-resolved, anti-correlated transitions in the Cy3 and Cy5 emission intensities (Fig. 5A). The resulting smFRET traces show well-defined, stochastic transitions between two distinct FRET states (Fig. 5B). The smFRET histogram in Fig. 5C shows that J11 exists as an equilibrium mixture of two populations, a large peak centered at a FRET value of 0.20 (σ = 0.10) and a smaller peak at 0.71 (σ = 0.19). Based on the similarities of the J11 peak locations to the assigned smFRET peaks for the A/B and A/C conformers, the low-FRET peak for J11 represents the A/C conformer, and the high-FRET peak corresponds to the A/B conformer. J11 represents the first identified 3WJ that can stably populate the A/B and A/C conformers. The slightly lower median FRET value and larger width of the high FRET population compared to that observed for J1 suggests that domain C for the A/B conformer of J11 is in a more open position (larger interdomain angle θ) and has greater conformational flexibility than the J1 conformer.

The transitions in the smFRET traces indicate that J11 unfolds to the open conformation and then refolds into one of the conformers as a stochastic process. The lack of a middle FRET population suggests that although refolding may occur through the open conformation, it is an on-pathway intermediate that is not measurably populated on our observation timescale (100-ms resolution). To determine the conformer transition rates, cumulative, dwell-time histograms were constructed from the measured durations of individual transition events (Fig. 5D). Fitting the histograms with single-exponential rate equations (Eq. (5)) gives conformer transition rates of $k_{A/C \rightarrow A/B} = 0.49\,s^{-1}$ and $k_{A/B \rightarrow A/C} = 2.51\,s^{-1}$. These rates correspond to lifetimes of ~ 2 s for the A/C conformer and 0.4 s for the A/B conformer. From the rates, an equilibrium constant of the A/B conformer relative to the A/C conformer is calculated as $K_{eq} = {k_{A/C \rightarrow A/B}}/{k_{A/B \rightarrow A/C}}$ and yields a value K_{eq} of 0.2. According to $\Delta G^o = -RTlnK_{eq}$, this equilibrium value reflects a free energy difference of ~1 kcal/mol between the two stacked conformations. Fig. 6 illustrates the energetic and domain-stacking differences for J11 with the A/C conformer as the more energetically favorable state.

With insight from the smFRET experiments that J11 can exist as an interconverting population of A/B and A/C conformers at 10 mM Mg^{2+}, the ensemble FRET (E_{FRET}) value for J11 should represent a mixture of the E_{FRET} values for the A/B and A/C junctions. To test this, the E_{FRET} value for J11 was treated as a conformer fraction-weighted, linear combination of the E_{FRET} values for J1 and J3. This analysis gives an A/C conformer fraction of 0.4 and a K_{eq} of 0.6, which is comparable to the direct observation by smFRET, highlighting the capability of single-

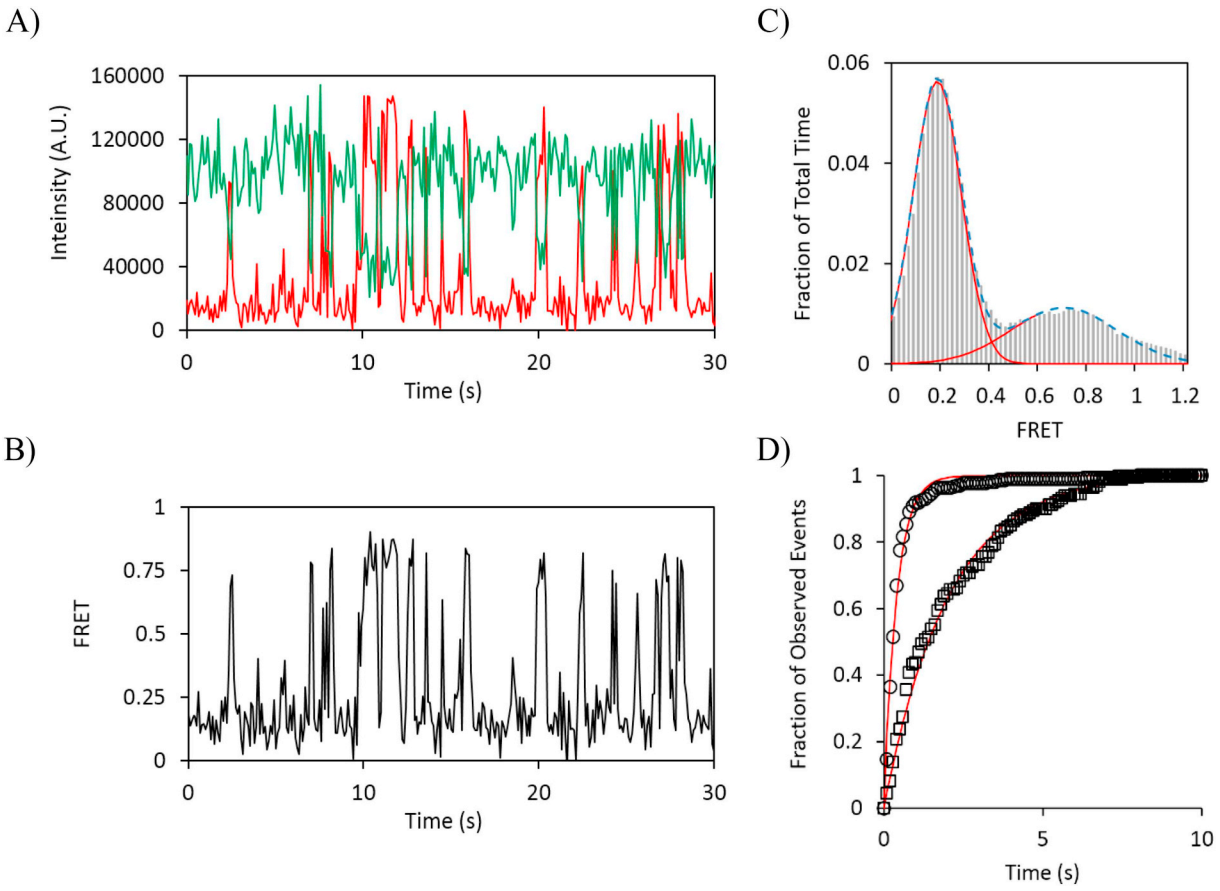

Fig. 5. Single-molecule FRET analysis of J11. A) Representative time trace showing the Cy3 and Cy5 intensities. B) smFRET trace determined from intensity traces by Eq. (4). C) The smFRET histogram for J11 (N_{mol} = 163). The red lines represent the two-peak Gaussian fit to the histogram, and the blue line is the cumulative fit ($R^2 > 0.99$). D) Normalized, cumulative dwell-time histograms for the A/C (open squares) and A/B (open circles) conformers. The solid red lines represent the best fits by single exponential rate equations (Eq. (5)), yielding rate constants of $k_{A/C \rightarrow A/B} = 0.49\ s^{-1}$ and $k_{A/B \rightarrow A/C} = 2.51\ s^{-1}$. (For interpretation of the references to colour in this figure legend, the reader is referred to the web version of this article.)

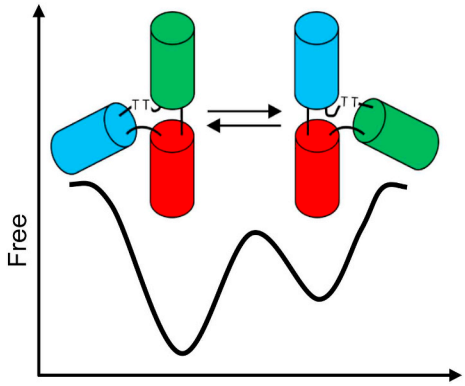

Fig. 6. Free energy diagram illustrating the relative positions of the three domains for the A/C and A/B conformers and their free energy differences for J11. The cylinders represent the helical domains with the same colour scheme as in Fig. 1.

molecule methods to detect multiple populations and resolve ensemble values.

Previous work revealed that bulged 3WJs can sample different conformations on the nanosecond timescale in the absence of divalent metal ions [34,35]. The findings here further demonstrate the stabilizing effect of divalent metal ions on the folding behavior of structured nucleic acids [39,53,59,60]. Mg^{2+} stabilizes DNA 3WJ conformers but can permit structural rearrangements that switch the helical stacking partners. Interestingly, the observed interconversion rates for J11 are comparable to the transition rates observed in 4WJs that involve the exchange of stacking partners under similar Mg^{2+} concentrations [39,42,52]. The presence of the bulge domain likely increases the flexibility at the junction, and these unpaired nucleotides participate in stacking interactions within the core that specify the preferred stacked conformers.

4. Conclusions

DNA nanostructure formation relies on the accurate self-assembly of single-stranded DNA into ordered domains that become organized into complex, three-dimensional structures [10]. Helical junctions, such as 3WJs and 4WJs, serve architectural roles to arrange and stabilize these domains. The work presented here shows that 3WJs can also be dynamic elements and that the presence of a small single-stranded domain can enhance the conformational entropy of 3WJs. The insertion of bulge domains within the 3WJ core allows the junction to switch between two globally similar conformations that differ according to the identities of the coaxially stacked domains. The sensitivity of conformer selection by the 3WJs to the core and bulge sequences indicates that additional work is required to develop more robust understanding of the complex interactions among the terminal and penultimate base pairs and the bulge nucleotides. 3WJs can be engineered such that the interdomain angles, coaxially stacking partners, and conformational switching behavior can be specified by the sequence design of the junction. In addition, the findings further illustrate how single-stranded domains can expand the structural capabilities of helical domains and

will support improvements in the folding principles that guide the rational design of functional DNA nanostructures.

Acknowledgements

This work was supported by start-up funds from Loyola University Chicago to B.C.

Conflicts of interest

All authors declare no conflicts of interest in this paper

Appendix A. Supplementary data

Supplementary data to this article can be found online at https://doi.org/10.1016/j.bpc.2018.12.001.

References

[1] E. Bonneau, N. Girard, S. Lemieux, P. Legault, The NMR structure of the II-III-VI three-way junction from the Neurospora VS ribozyme reveals a critical tertiary interaction and provides new insights into the global ribozyme structure, RNA 21 (2015) 1621–1632.
[2] D. Klostermeier, D.P. Millar, Helical junctions as determinants for RNA folding: origin of tertiary structure stability of the hairpin ribozyme, Biochemistry 39 (2000) 12970–12978.
[3] G.S. Bassi, A.I. Murchie, F. Walter, R.M. Clegg, D.M. Lilley, Ion-induced folding of the hammerhead ribozyme: a fluorescence resonance energy transfer study, EMBO J. 16 (1997) 7481–7489.
[4] S. Mohan, H.F. Noller, Recurring RNA structural motifs underlie the mechanics of L1 stalk movement, Nat. Commun. 8 (2017) 14285.
[5] K. Réblová, J. Sponer, F. Lankas, Structure and mechanical properties of the ribosomal L1 stalk three-way junction, Nucleic Acids Res. 40 (2012) 6290–6303.
[6] J. Ouellet, S. Melcher, A. Iqbal, Y. Ding, D.M. Lilley, Structure of the three-way helical junction of the hepatitis C virus IRES element, RNA 16 (2010) 1597–1609.
[7] K.C. Woods, S.S. Martin, V.C. Chu, E.P. Baldwin, Quasi-equivalence in site-specific recombinase structure and function: crystal structure and activity of trimeric Cre recombinase bound to a three-way Lox DNA junction, J. Mol. Biol. 313 (2001) 49–69.
[8] W.A. Rosche, T.Q. Trinh, R.R. Sinden, Differential DNA secondary structure-mediated deletion mutation in the leading and lagging strands, J. Bacteriol. 177 (1995) 4385–4391.
[9] M.M. Slean, K. Reddy, B. Wu, K. Nichol Edamura, M. Kekis, F.H. Nelissen, R.L. Aspers, M. Tessari, O.D. Schärer, S.S. Wijmenga, C.E. Pearson, Interconverting conformations of slipped-DNA junctions formed by trinucleotide repeats affect repair outcome, Biochemistry 52 (2013) 773–785.
[10] L. Jaeger, A. Chworos, The architectonics of programmable RNA and DNA nanostructures, Curr. Opin. Struct. Biol. 16 (2006) 531–543.
[11] F. Zhang, S. Jiang, S. Wu, Y. Li, C. Mao, Y. Liu, H. Yan, Complex wireframe DNA origami nanostructures with multi-arm junction vertices, Nat. Nanotechnol. 10 (2015) 779–784.
[12] F. Li, Y. Lin, X.C. Le, Binding-induced formation of DNA three-way junctions and its application to protein detection and DNA strand displacement, Anal. Chem. 85 (2013) 10835–10841.
[13] Y. Xu, X. Bian, Y. Sang, Y. Li, D. Li, W. Cheng, Y. Yin, H. Ju, S. Ding, Bis-three-way junction nanostructure and DNA machineries for ultrasensitive and specific detection of BCR/ABL fusion gene by chemiluminescence imaging, Sci. Rep. 6 (2016) 32370.
[14] S.M. Taghdisi, N.M. Danesh, M. Ramezani, R. Yazdian-Robati, K. Abnous, A Novel AS1411 aptamer-based three-way junction pocket DNA nanostructure loaded with doxorubicin for targeting cancer cells in vitro and in vivo, Mol. Pharm. 15 (2018) 1972–1978.
[15] D.R. Duckett, D.M. Lilley, The three-way DNA junction is a Y-shaped molecule in which there is no helix-helix stacking, EMBO J. 9 (1990) 1659–1664.
[16] A. Toulmin, L.E. Baltierra-Jasso, M.J. Morten, T. Sabir, P. McGlynn, G.F. Schröder, B.O. Smith, S.W. Magennis, Conformational heterogeneity in a fully complementary DNA three-way junction with a GC-rich branchpoint, Biochemistry 56 (2017) 4985–4991.
[17] T. Sabir, A. Toulmin, L. Ma, A.C. Jones, P. McGlynn, G.F. Schröder, S.W. Magennis, Branchpoint expansion in a fully complementary three-way DNA junction, J. Am. Chem. Soc. 134 (2012) 6280–6285.
[18] R.I. Ma, N.R. Kallenbach, R.D. Sheardy, M.L. Petrillo, N.C. Seeman, Three-arm nucleic acid junctions are flexible, Nucleic Acids Res. 14 (1986) 9745–9753.
[19] J. Santalucia, D. Hicks, The thermodynamics of DNA structural motifs, Annu. Rev. Biophys. Biomol. Struct. 33 (2004) 415–440.
[20] T. Tran, B. Cannon, Differential effects of strand asymmetry on the energetics and structural flexibility of DNA internal loops, Biochemistry 56 (2017) 6448–6459.
[21] B.N. Bourdélat-Parks, R.M. Wartell, Thermodynamic stability of DNA tandem mismatches, Biochemistry 43 (2004) 9918–9925.
[22] S.J. Schroeder, D.H. Turner, Factors affecting the thermodynamic stability of small asymmetric internal loops in RNA, Biochemistry 39 (2000) 9257–9274.
[23] D.H. Mathews, J. Sabina, M. Zuker, D.H. Turner, Expanded sequence dependence of thermodynamic parameters improves prediction of RNA secondary structure, J. Mol. Biol. 288 (1999) 911–940.
[24] X. Shi, K.A. Beauchamp, P.B. Harbury, D. Herschlag, From a structural average to the conformational ensemble of a DNA bulge, Proc. Natl. Acad. Sci. U. S. A. 111 (2014) E1473–E1480.
[25] C. Gohlke, A.I. Murchie, D.M. Lilley, R.M. Clegg, Kinking of DNA and RNA helices by bulged nucleotides observed by fluorescence resonance energy transfer, Proc. Natl. Acad. Sci. U. S. A. 91 (1994) 11660–11664.
[26] A.K. Wozniak, G.F. Schröder, H. Grubmüller, C.A. Seidel, F. Oesterhelt, Single-molecule FRET measures bends and kinks in DNA, Proc. Natl. Acad. Sci. U. S. A. 105 (2008) 18337–18342.
[27] J.B. Welch, F. Walter, D.M. Lilley, Two inequivalent folding isomers of the three-way DNA junction with unpaired bases: sequence-dependence of the folded conformation, J. Mol. Biol. 251 (1995) 507–519.
[28] M.A. Rosen, D.J. Patel, Structural features of a three-stranded DNA junction containing a C-C junctional bulge, Biochemistry 32 (1993) 6576–6587.
[29] B.N. van Buuren, F.J. Overmars, J.H. Ippel, C. Altona, S.S. Wijmenga, Solution structure of a DNA three-way junction containing two unpaired thymidine bases. Identification of sequence features that decide conformer selection, J. Mol. Biol. 304 (2000) 371–383.
[30] N.B. Leontis, M.T. Hills, M. Piotto, I.V. Ouporov, A. Malhotra, D.G. Gorenstein, Helical stacking in DNA three-way junctions containing two unpaired pyrimidines: proton NMR studies, Biophys. J. 68 (1995) 251–265.
[31] F.J. Overmars, J.A. Pikkemaat, H. van den Elst, J.H. van Boom, C. Altona, NMR studies of DNA three-way junctions containing two unpaired thymidine bases: the influence of the sequence at the junction on the stability of the stacking conformers, J. Mol. Biol. 255 (1996) 702–713.
[32] J.B. Welch, D.R. Duckett, D.M. Lilley, Structures of bulged three-way DNA junctions, Nucleic Acids Res. 21 (1993) 4548–4555.
[33] C.E. Carr, L.A. Marky, Increased flexibility between stems of intramolecular three-way junctions by the insertion of bulges, Biophys. J. 114 (2018) 2764–2774.
[34] R.M. Young, A.P. Singh, A.K. Thazhathveetil, V.Y. Cho, Y. Zhang, N. Renaud, F.C. Grozema, D.N. Beratan, M.A. Ratner, G.C. Schatz, Y.A. Berlin, F.D. Lewis, M.R. Wasielewski, Charge transport across DNA-based three-way junctions, J. Am. Chem. Soc. 137 (2015) 5113–5122.
[35] Y. Zhang, R.M. Young, A.K. Thazhathveetil, A.P. Singh, C. Liu, Y.A. Berlin, F.C. Grozema, F.D. Lewis, M.A. Ratner, N. Renaud, K. Siriwong, A.A. Voityuk, M.R. Wasielewski, D.N. Beratan, Conformationally gated charge transfer in DNA three-way junctions, J. Phys. Chem. Lett. 6 (2015) 2434–2438.
[36] S. Muhuri, K. Mimura, D. Miyoshi, N. Sugimoto, Stabilization of three-way junctions of DNA under molecular crowding conditions, J. Am. Chem. Soc. 131 (2009) 9268–9280.
[37] R. Assenberg, A. Weston, D.L. Cardy, K.R. Fox, Sequence-dependent folding of DNA three-way junctions, Nucleic Acids Res. 30 (2002) 5142–5150.
[38] S.A. McKinney, A.D. Freeman, D.M. Lilley, T. Ha, Observing spontaneous branch migration of Holliday junctions one step at a time, Proc. Natl. Acad. Sci. U. S. A. 102 (2005) 5715–5720.
[39] S.A. McKinney, A.C. Déclais, D.M. Lilley, T. Ha, Structural dynamics of individual Holliday junctions, Nat. Struct. Biol. 10 (2003) 93–97.
[40] B. Cannon, A.H. Kachroo, I. Jarmoskaite, M. Jayaram, R. Russell, Hexapeptides that inhibit processing of branched DNA structures induce a dynamic ensemble of holliday junction conformations, J. Biol. Chem. 290 (2015) 22734–22746.
[41] M. Karymov, D. Daniel, O.F. Sankey, Y.L. Lyubchenko, Holliday junction dynamics and branch migration: single-molecule analysis, Proc. Natl. Acad. Sci. U. S. A. 102 (2005) 8186–8191.
[42] S. Hohng, C. Joo, T. Ha, Single-molecule three-color FRET, Biophys. J. 87 (2004) 1328–1337.
[43] D.A. Erie, K.R. Weninger, Single molecule studies of DNA mismatch repair, DNA Repair (Amst) 20 (2014) 71–81.
[44] C. Bustamante, W. Cheng, Y.X. Mejia, Y.X. Meija, Revisiting the central dogma one molecule at a time, Cell 144 (2011) 480–497.
[45] G. Bokinsky, D. Rueda, V.K. Misra, M.M. Rhodes, A. Gordus, H.P. Babcock, N.G. Walter, X. Zhuang, Single-molecule transition-state analysis of RNA folding, Proc. Natl. Acad. Sci. U. S. A. 100 (2003) 9302–9307.
[46] X. Zhuang, L.E. Bartley, H.P. Babcock, R. Russell, T. Ha, D. Herschlag, S. Chu, A single-molecule study of RNA catalysis and folding, Science 288 (2000) 2048–2051.
[47] M.T. Woodside, P.C. Anthony, W.M. Behnke-Parks, K. Larizadeh, D. Herschlag, S.M. Block, Direct measurement of the full, sequence-dependent folding landscape of a nucleic acid, Science 314 (2006) 1001–1004.
[48] T. Ha, Single-molecule fluorescence resonance energy transfer, Methods 25 (2001) 78–86.
[49] R.M. Clegg, A.I. Murchie, A. Zechel, C. Carlberg, S. Diekmann, D.M. Lilley, Fluorescence resonance energy transfer analysis of the structure of the four-way DNA junction, Biochemistry 31 (1992) 4846–4856.
[50] J. Malicka, I. Gryczynski, J. Kusba, J.R. Lakowicz, Effects of metallic silver island films on resonance energy transfer between N,N'-(dipropyl)-tetramethyl- indocarbocyanine (Cy3)- and N,N'-(dipropyl)-tetramethyl- indodicarbocyanine (Cy5)-labeled DNA, Biopolymers 70 (2003) 595–603.
[51] R. Sreenivasan, S. Heitkamp, M. Chhabra, R. Saecker, E. Lingeman, M. Poulos, D. McCaslin, M.W. Capp, I. Artsimovitch, M.T. Record, Fluorescence resonance energy transfer characterization of DNA wrapping in closed and open *Escherichia coli* RNA polymerase-λP(R) promoter complexes, Biochemistry 55 (2016) 2174–2186.
[52] B. Cannon, A.H. Kachroo, I. Jarmoskaite, M. Jayaram, R. Russell, Hexapeptides that

inhibit processing of branched DNA structures induce a dynamic ensemble of Holliday junction conformations, J. Biol. Chem. 290 (2015) 22734–22746.
[53] D. Leipply, D. Lambert, D.E. Draper, Ion-RNA interactions thermodynamic analysis of the effects of mono- and divalent ions on RNA conformational equilibria, Methods Enzymol. 469 (2009) 433–463.
[54] B. Wu, F. Girard, B. van Buuren, J. Schleucher, M. Tessari, S. Wijmenga, Global structure of a DNA three-way junction by solution NMR: towards prediction of 3H fold, Nucleic Acids Res. 32 (2004) 3228–3239.
[55] N.E. Møllegaard, A.I. Murchie, D.M. Lilley, P.E. Nielsen, Uranyl photoprobing of a four-way DNA junction: evidence for specific metal ion binding, EMBO J. 13 (1994) 1508–1513.
[56] H. Zhang, J.A. Endrizzi, Y. Shu, F. Haque, C. Sauter, L.S. Shlyakhtenko, Y. Lyubchenko, P. Guo, Y.I. Chi, Crystal structure of 3WJ core revealing divalent ion-promoted thermostability and assembly of the Phi29 hexameric motor pRNA, RNA 19 (2013) 1226–1237.
[57] S. Strom, E. Shiskova, Y. Hahm, N. Grover, Thermodynamic examination of 1-to 5-nt purine bulge loops in RNA and DNA constructs, RNA 21 (2015) 1313–1322.
[58] N.L. Goddard, G. Bonnet, O. Krichevsky, A. Libchaber, Sequence dependent rigidity of single stranded DNA, Phys. Rev. Lett. 85 (2000) 2400–2403.
[59] A. Plumridge, A.M. Katz, G.D. Calvey, R. Elber, S. Kirmizialtin, L. Pollack, Revealing the distinct folding phases of an RNA three-helix junction, Nucleic Acids Res. 46 (2018) 7354–7365.
[60] H.D. Kim, G.U. Nienhaus, T. Ha, J.W. Orr, J.R. Williamson, S. Chu, Mg2+ −dependent conformational change of RNA studied by fluorescence correlation and FRET on immobilized single molecules, Proc. Natl. Acad. Sci. U. S. A. 99 (2002) 4284–4289.